Faraday Discussions

The Red Admiral butterfly's living light sensors and signals

Journal:	*Faraday Discussions*
Manuscript ID	FD-ART-06-2020-000075.R1
Article Type:	Paper
Date Submitted by the Author:	22-Jun-2020
Complete List of Authors:	Pirih, Primož; University of Ljubljana Biotechnical faculty, Biology Meglič, Andrej; University of Ljubljana, Eye Hospital, University Medical Centre Stavenga, Doekele; University of Groningen, Surfaces and thin films Arikawa, Kentaro; SOKENDAI, Evolutionary studies of biosystems Belušič, Gregor; University of Ljubljana Biotechnical faculty, Biology

Faraday Discussions

ROYAL SOCIETY OF CHEMISTRY

Revised manuscript

The Red Admiral Butterfly's Living Light Sensors and Signals

Primož Pirih*[a,b], Andrej Meglič[a,c], Doekele Stavenga[d], Kentaro Arikawa[e], Gregor Belušič[a]

Abstract

We studied the wing colouration and the compound eyes of Red admiral butterflies with optical methods. We measured reflectance spectra of the wing and scales of *Vanessa atalanta* and modelled the thin film reflectance of the wing membrane and the blue scales. We utilized the eyeshine in the compound eye of *Vanessa indica* to determine the spectral and polarisation characteristics of its optical sensor units, the ommatidia. Pupil responses were measured with a large-aperture optophysiological setup as reduction in the eyeshine reflection caused by monochromatic stimuli. Processing of spectral and polarisation responses of individual ommatidia revealed a random array with three types of ommatidia: about a tenth contain two blue-sensitive photoreceptors, 45% have two UV-sensitive photoreceptors and 45% have a mixed UV-blue pair. All types contain six green receptors and a basal photoreceptor. Optical modelling of the rhabdom suggests that the basal photoreceptors have a red-shifted sensitivity, which might enhance the Red admiral's ability for discriminating red colours on the wing. Under daylight conditions, the red shift of the basal photoreceptor is ~30 nm, compared to the rhodopsin spectrum template peaking at 520 nm, while the shift of green photoreceptors is ~15 nm.

Keywords: compound eye – rhabdom – spectral sensitivity – eyeshine – wing scale – photoreceptors

[ORCID[f]]

Introduction

Butterflies are universally recognized by their wealth of colour displays. Butterfly wings derive their colours from a dense coverage of scales, which overlap each other like tiles on a roof. Butterfly wing scales are basically a combination of two layers, an

a Department of Biology, University of Ljubljana, Slovenia
* Correspondence: primoz.pirih@gmail.com
b Votan d.o.o., Ljubljana, Slovenia
c Eye Hospital, University of Ljubljana Medical Centre, Slovenia
d Surfaces and thin films, ZIAM, University of Groningen, the Netherlands
e Laboratory of Neuroethology, Sokendai,-Hayama, Kanagawa, Japan
f ORCID ID: 0000-0003-1710-444X (PP), 0000-0003-3837-8108 (AM), 0000-0002-2518-6177 (DGS), 0000-0002-4365-0762 (KA), 0000-0003-3571-1948 (GB)

upper and a lower lamina[1,2]. The upper lamina consists of numerous parallel ridges connected by crossribs, while the lower lamina is almost a flat plate. Pigmentary colours in the scales are due to the deposited pigments that belong to chemical classes characteristic for the various butterfly families. For instance, the members of the Pieridae family employ pterins in their wing scales, the Papilionidae express papiliochromes, and the wing scales of Nymphalidae feature various ommochromes and their precursor 3-hydroxykynurenine[3,4,5]. Yet, because of the nanosized dimensions of the scale elements, the colours of many butterfly species are structurally determined. The iconic *Morpho* butterflies, for instance, have brilliant blue wings due to ridge structures that function as optical multilayers. The blue eyespots of peacock butterflies are due to unpigmented scales with a lower lamina acting as a thin film blue reflector, while the colour of scales of various lycaenids and papilionids is due to gyroid nanostructures[6,7,8,9,10].

Their rich gamut of wing colouration is paralleled with an equal richness of colour vision capacities. It is becoming apparent that butterfly vision can employ many spectrally distinct photoreceptors. For instance, the Asian Swallowtail *Papilio xuthus* has tetrachromatic vision, presumably based on four of the eight spectral types of photoreceptors[11]. Possibly more diverse colour vision systems exist, since a recent study on another papilionid, *Graphium sarpedon*, revealed 15 types of photoreceptors[12]. On the other hand, butterflies can also have only three types of photoreceptors peaking in the ultraviolet, blue and green wavelength range, respectively[13], like the honeybee[14,15]. The diversity of spectral receptors presumably enhances the visual detection of conspecifics, and it has been proposed that the spectral characteristics of the retina may be tuned to wing colouration[16,17,18,19].

Figure 1. Red admiral's wings and its compound eye. (a) The Red admiral *Vanessa atalanta* drinking nectar from *Sakura* cherry blossom (after hibernation, March 2020, Ljubljana, Slovenia). **(b)** The Red admirals *Vanessa atalanta* and *V. indica*. **(c)** The eyeshine of the central frontal eye of the Indian red admiral, *Vanessa indica*. The intact peripheral ommatidia are orange, the central ommatidia are pale due to bleaching. The periodicity of the ommatidial lattice is ~25 µm.

Here, we investigate the spectral properties of the wings and compound eyes of two closely related species of nymphalid butterflies, *Vanessa atalanta* and *Vanessa indica* (Fig. 1b,c). The dorsal and ventral sides of wings of these Red admirals are marked by red bands together with white and blue spots surrounded by large black areas (Fig. 1a,b). We characterize the wing reflectance spectra and relate them to the spectral properties of

the compound eyes. For the compound eye studies, we developed a special-built imaging spectrophotometry setup[30], and used it with a novel optophysiological method for an *in vivo* large-scale analysis of photoreceptor characteristics, utilising the eyeshine (Fig. 1c) and the pupil mechanism. The method bears conceptual similarity with extracellular electroretinography (ERG), justifying the name optical retinography (ORG).

Reflections on the wing

Spectrophotometric measurements of wings and wing scales were performed on *Vanessa atalanta*, captured near Groningen, the Netherlands. The reflectance and transmittance spectra of wing scales were measured with a microspectrophotometer, and for the reflectance spectra of the intact wing a bifurcated reflection probe and spectrometer (Avantes, Apeldoorn, Netherlands) was used. The measurement techniques have been described in detail before[20].

The wings of *Vanessa atalanta* are generally rather dark, but prominent red, blue and white areas exist. The colouration is due to stacks of scales on the wings (Fig. 2a). The anatomy of the scales is basic, with parallel ridges connected by crossribs, leaving large windows in the upper lamina, through which the lower lamina can be seen (Fig. 2b). Incident light is partly scattered by the ridges and crossribs, but a major part travels through the windows and, when reaching the lower lamina, is partly reflected there. When the light that proceeds through the lower lamina reaches the wing substrate, it is partly reflected and can travel back and add to the total reflection.

The reflections from the lower lamina can be studied on blue unpigmented scales *in situ*, on the wing (Fig. 2a). The adwing, lower side of the blue scales has a highly metallic appearance, because it is a thin plate, which by interference strongly reflects in the blue wavelength range (Fig. 2e). A blue scale observed from the abwing, upper side has a more subdued appearance, because of the scattering upper lamina (Fig. 2f). Thin film modelling shows that the thickness of the lower lamina of these scales is about 220 nm (Fig. 2c, *lower dotted curve*). The reflectance spectrum measured from a blue scale *in situ*, on the wing, is raised with respect to the ideal thin film spectrum because of the contribution of the upper lamina scattering and the wing reflections (Fig. 2c, *middle solid curve*). This effect is even stronger when measuring the reflectance from a stack of blue scales (Fig. 2c, upper *dash-dot curve*). Hence, the stacked blue scales create together the whitish wing patches (Fig. 1a-c), but in the clearly blue areas the cover scales on top of the scale stack are blue and unpigmented, while the underlying ground scales are heavily pigmented with melanin and do not add to the reflections.

When the scales are removed, reflectance spectra of the naked wing show oscillations, which also exhibit a thin film behaviour (Fig. 2d). The measured spectrum (Fig. 2d, *solid curve*) closely corresponds with the reflectance spectrum calculated for a slightly varying thin film, with mean thickness 2.50 µm and standard deviation 70 nm (Fig. 2d, *dotted curve*).

The red scales (Fig. 2g) contain a substantial amount of short-wavelength absorbing ommochrome pigment, as follows from the transmittance spectrum measured from an

isolated scale in immersion oil (Fig. 2h, *upper dashed curve*). As a consequence, in the reflectance spectrum measured from a red scale on the wing, the thin film reflections of the lower lamina are no longer apparent (Fig. 2h, *lower solid curve*). The scale's reflectance in the blue is heavily suppressed, and what remains is due to the upper lamina, the lower lamina reflections in the long-wavelength range, as well as the reflections by the wing proper. The long-wavelength reflectance is augmented when the red scales are stacked (Fig. 2h, *middle dash-dot curve*).

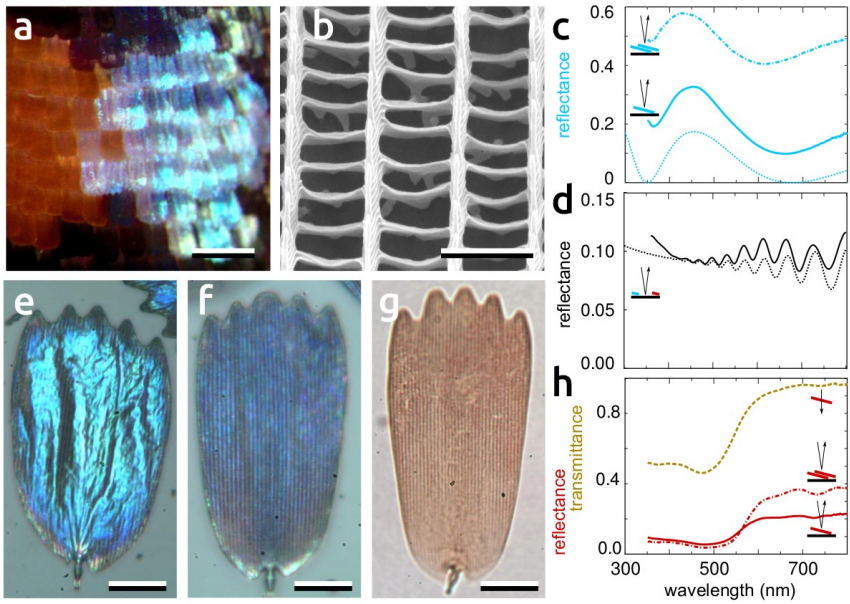

Figure 2. Optics of Red admiral's wing scales. (a) The lattice of wing scales at the ventral forewing of *V. atalanta* with red, black and blue scales. **(b)** SEM of a red scale. **(c)** Measured reflectance spectra of a single blue scale on the wing (middle curve), and of two blue scales stacked on top of each other on the wing (upper curve), and a model for a chitinous thin film with thickness 220 nm (lower curve). **(d)** Measured reflectance spectra of a clear wing (solid curve) and a model of a chitinous thin film with Gaussian distributed thickness, mean 2.5 µm, standard deviation 70 nm. **(e)** A blue scale observed from the adwing, lower side scale. **(f)** A blue scale observed from the abwing, upper side. (g) A red scale. Scale bars: (a) 200 µm, (b) 2 µm, (e-g) 20 µm

Reflections on the eye

In butterfly ommatidia waveguides are central

Like in other arthropods, butterfly compound eyes consist of discrete building blocks, the ommatidia. Butterfly ommatidia contain nine photoreceptor cells, whose distinct spectral sensitivities are chiefly determined by the absorption spectrum of the UV, blue or green-peaking visual pigment, rhodopsin, expressed in a special cell organelle, the rhabdomere. In a butterfly ommatidium, the nine rhabdomeres are closely apposed, forming a fused rhabdom, a cylindrical structure that acts as an optical waveguide. The spectral sensitivity of photoreceptors is modified by self-screening and

by screening by the visual pigments contained in the apposed rhabdomeres. In many butterflies, additional yellow and red screening pigment granules, located in the photoreceptor cell bodies near the rhabdom, function as spectral filters. The photoreceptor spectral types may also differ between females and males and their diversity may be enriched by expression of multiple visual pigments in a single photoreceptor[12,21,22,23,24,25].

Methods for studying spectral sensitivities

Characterisation of the molecular identity of the visual pigment, while extremely valuable, cannot accurately predict the effective spectral sensitivity of a photoreceptor. The gold standard for assessing the *in vivo* spectral sensitivity of photoreceptors thus remains intracellular electrophysiology. Localisation and identification of recorded cells however requires painstaking anatomical efforts, where at most a few cells can be identified in one preparation[12,21,25,26,27,28].

An attractive alternative approach is the application of *in vivo* optical methods, useful in a large number of butterfly species that have a tapetal reflector below the rhabdom. Epi-illumination of the compound eyes then creates an eyeshine. This phenomenon immediately reveals that the ommatidia of many butterfly eyes are not uniform but heterogeneous[21,29,30,31,32]. Furthermore, the eyeshine allows for *in vivo* spectroscopy studies of visual pigments[16,33,34,35,36] and of the screening pigments[37]. A special bonus is provided by the pupil mechanism, the assembly of mobile pigment granules existing in the photoreceptor cell bodies. At low illumination intensities the granules reside away from the rhabdom boundary, but upon illumination they migrate toward the rhabdom[34,38,39,40]. By measuring the change in eyeshine intensity in response to monochromatic stimuli, the spectral sensitivity of the pupil mechanism, and thus that of the photoreceptors in an ommatidium, can be assessed.

The compound eye of nymphalid butterflies

The Red admirals belong to the genus *Vanessa* of the tribe Nymphalini. Their eyes contain ommatidia with three spectrally distinct photoreceptors peaking in the UV, blue and green, respectively[13,26,41,42,43], enabling trichromatic colour vision with a range that is, compared to human colour vision, shifted towards the UV. The general eye structure seems to be shared across the family Nymphalidae, except that the red screening pigments, present in a subset of ommatidia in some other tribes, e.g. Satyrini, Danaini and Heliconiini[27,30], have not been found in the eyes of the Nymphalini tribe. For the interpretation of the results of our optical measurements, we shall first summarize the current knowledge of the eye anatomy[27,38,39,41,42,44] and optics[30,40,45,46,47] in the family Nymphalidae (Fig. 3).

Incident light from a narrow spatial angle (1°-2°) is launched into the fused rhabdom waveguide by the corneal facet lens and a crystalline cone, which acts as a gradient index (GRIN) lens (Fig. 3a). Off-axis light is blocked by screening pigment in the primary and secondary pigment cells that surround the dioptric system as well as the photoreceptor cell bodies that stretch the length of the ommatidium, typically 300-450 µm. Inside the cell bodies, pigment granules reside remote from the rhabdom in the

dark-adapted state (Fig. 3a, DA, left side) and close to the rhabdom in the light-adapted state (Fig. 3a, LA, right side).

The rhabdomeres, together composing the rhabdom, consist of stacks of microvilli, tube-shaped structures bound by the lipid membrane harbouring visual pigment molecules. The rhabdomeres of the ultraviolet (UV) and blue (B) sensitive photoreceptors (R1,2) extend to about halfway the ommatidia, while the green (G) cells (R3-8) stretch the full length (as summarized in Fig. 3d). The rhabdomeric microvilli of a ninth photoreceptor (R9) are restricted proximally, near the tapetal reflector, which is formed from a convoluted tracheole and acts as a chirped optical multilayer (Fig. 3b). The spectral sensitivity of the R9 cell so far remains an enigma. The various photoreceptors are arranged as depicted in Fig. 3c, with the cell bodies of R1 and R2 directed parallel to the dorsoventral or vertical axis of the eye, R3 and R4 are oriented horizontally, and R5-8 diagonally (see also Fig. 3e). The extended rhabdomeric microvilli participate in principle in the rhabdom along the direction of their cell somata; the R9 cell is vertical and has a bilobed rhabdomere.

The ommatidia in the central eye part are anatomically similar to each other, but due to the opsin expression pattern and physiological properties there are three ommatidial types (Fig. 3f). The photoreceptors R1 and R2 form a mixed pair (UB, type I), are both UV sensitive (UU, type II), or are both blue sensitive (BB, type III). At the proximal level, two axons belonging to cells R1-2 and eight tracheolar tubes between the photoreceptors and the secondary pigment (glia) cells surround the photoreceptors, including the bilobed basal R9 (Fig. 3g).

Due to their structure, the microvilli are intrinsically dichroic, and as a consequence the photoreceptors are polarisation sensitive[48,49]. Effective polarisation sensitivity of the photoreceptor can be reduced by randomizing the orientation of the microvilli or it can be augmented by aligning the absorption dipoles of the visual pigment molecules[50]. The visual pigment molecules are embedded in the microvillar membrane and trigger the phototransduction process upon photon absorption. Interestingly, anatomical studies revealed that some R1-2 photoreceptors have bundles of microvilli in two alternating orientations away from the dorso-frontal axis, while the microvilli of other photoreceptors are aligned with that axis[27,38]. Intracellular measurements suggest a general picture that R1-2 cells are maximally sensitive to vertically, R3-4 to horizontally, and R5-8 to diagonally polarised light, respectively[26,27].

The light flux travelling in the rhabdom is partially absorbed by the visual pigments residing in the rhabdomeres. Absorption depends on various optical effects, like mutual filtering among the apposed rhabdomeres and the propagation of the light flux in the rhabdom in waveguide modes. Two waveguide modes are primarily present, the first resembling a Gaussian, and the second creating a doughnut like pattern[45,46]. The waveguide modes extend into the cell soma as a boundary wave, and part of that light flux can be absorbed by the mobile photoreceptor pigment granules, when pulled by the pupil mechanism toward the rhabdom from their dark-adapted (DA) to the light-adapted (LA) state (Fig. 3h,j). The light that escapes absorption and reaches the end of the rhabdom can be reflected back into the rhabdom by the tapetal mirror (Fig. 3k). The reflected light that is not absorbed on the way back, leaves the eye and then cannot only

be observed as the eyeshine, but it can also be exploited to discover the secrets of the inner eye.

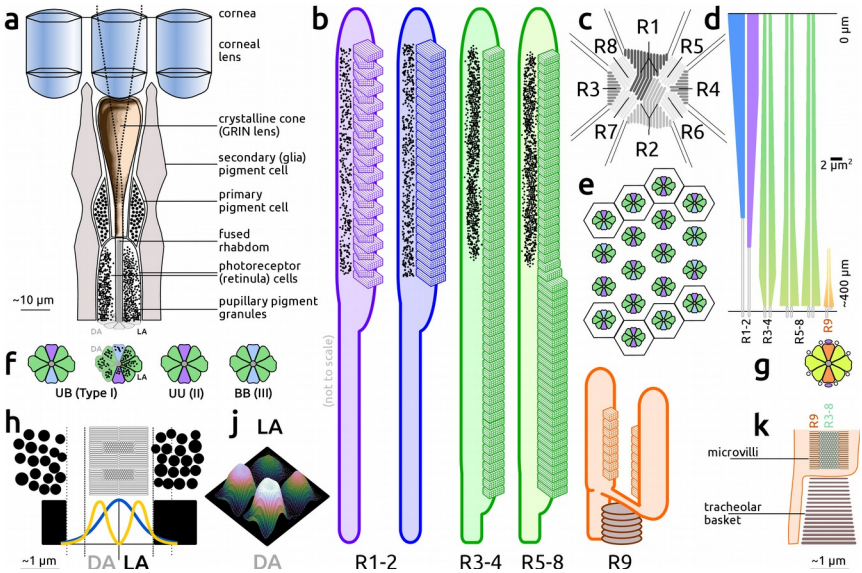

Figure 3. Optics of nymphalid butterfly eye. (a) Facet lenses and the distal part of a butterfly ommatidium. **(b)** Diagrams of the nine photoreceptor cells R1-9 (not to scale). **(c)** Cross-section of the photoreceptors R1-8 contributing rhabdomeres distally to the central rhabdom. **(d)** The R1,2 rhabdomeres are restricted to the distal part, R3-8 stretch the whole length of the ommatidium, and the bilobed R9 rhabdomere exists proximally. **(e)** Arrangement of ommatidia in a hexagonal lattice. **(f)** Three ommatidial types make four different combinations of U (ultraviolet) and B (blue) receptors. **(g)** Diagram of a proximal section of an ommatidium with tracheoles. **(h)** Pupillary pigment granules remote from the rhabdom in the dark-adapted (DA) state and close to the rhabdom in the light-adapted (LA) state, then interacting with the boundary wave of the optical waveguide modes. **(j)** Profiles of the radiation diagrams as a function of adaptation. **(k)** Basket of tracheoles reflecting light back into the rhabdom, which consists of microvilli. For details, see text.

Optical retinography (ORG)

For studying the eyeshine, we have built an optical system, which is essentially an epi-illumination microscope[30] with a shortened, telescopic tube and additional stops (Fig. 4). A female Indian red admiral, *Vanessa indica*, was captured in Hayama, Japan, immobilized into a shrink tube using beeswax, and put to a goniometric stage so that its eye centre was in the focal point of the main objective lens. The positions of lenses in the observation beams were adjusted to image the corneal plane. Illumination and observation field stops were stopped down to minimize scattered light and the corneal stop selected the set of ommatidia for bleaching (Fig. 4c, d3,d4,d2). The stacks with eyeshine images acquired during the stimulation protocols (SI, Fig. S1) were imported into ImageJ/Fiji[51], corrected for background and registered to the reference image using plugins bUnwarpJ[52] and StackReg[53]. The mean grey value data from 628 ommatidia were exported to GNU Octave[54] and converted to log reflectance values using dark-adapted reference grey values obtained from the same ommatidia. For further details on

the setup, calibration, stimulation protocols and image analysis, see Supplementary Information.

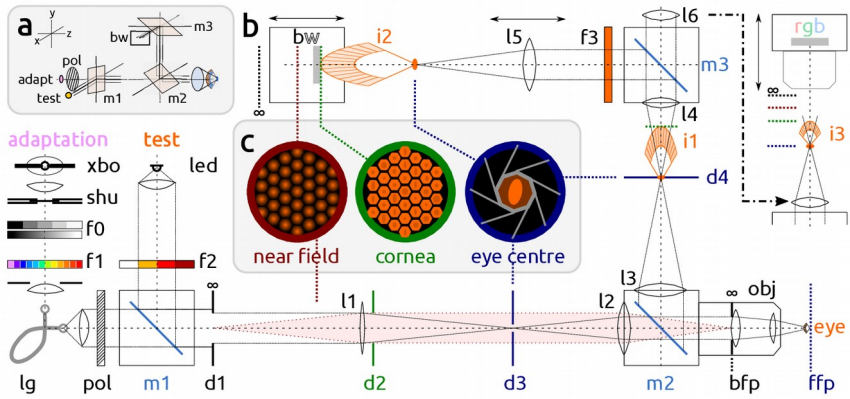

Figure 4. Epi-illumination telemicroscope setup for optical retinography of butterfly eyeshine. (a) Condensed diagram of the setup. (b) Optical arrangement of the setup, consisting of an adaptation and test beam, focused at the butterfly eye, and the reflected beam, which is observed with an RGB camera and measured with a monochrome camera. (c) Schematic appearance of the eyeshine at different z-planes.

Static eyeshine

We studied *Vanessa*'s compound eyes by first assessing the spectral characteristics of the tapetal mirror. We estimate that each compound eye contains ~10.000 ommatidia, as in other similarly sized butterflies, and that we have imaged around 10% of them in the central part of the eye (Fig. 5a). As shown in Fig. 1c, the eyeshine is generally strongly affected by the visual pigments. To better reveal the tapetal multilayer, the central part of the observed eye part was exposed for several hours to intermittent flashes of orange light that bleached the main, green visual pigment (SI Fig. S1b). After a short dark period during which the pupillary granules travelled to their dark-adapted location, we took monochrome images in the range 400-700 nm. The images are shown inverted: reflecting ommatidia appear black (Fig. 5b,c). The reflectance of the ommatidia clearly differs between the bleached and unbleached ommatidia at wavelengths <600 nm, because the visual pigments strongly absorb the light flux travelling in the rhabdom in that wavelength range (Fig. 5c). The bleached ommatidia reflect about uniformly between 520 nm and 620 nm. In the red wavelength range, where the visual pigments absorption is negligible, some ommatidia stop reflecting at 640 nm and only a small fraction reflects at ≥ 660 nm (dark spots in Fig. 5b). The unbleached ommatidia on the perimeter reflect less than the bleached ommatidia in the range between 400 nm and 560 nm (Fig. 5c, SI Fig. S1c). Interestingly, a heterogeneous ommatidial mosaic appears at 460 nm.

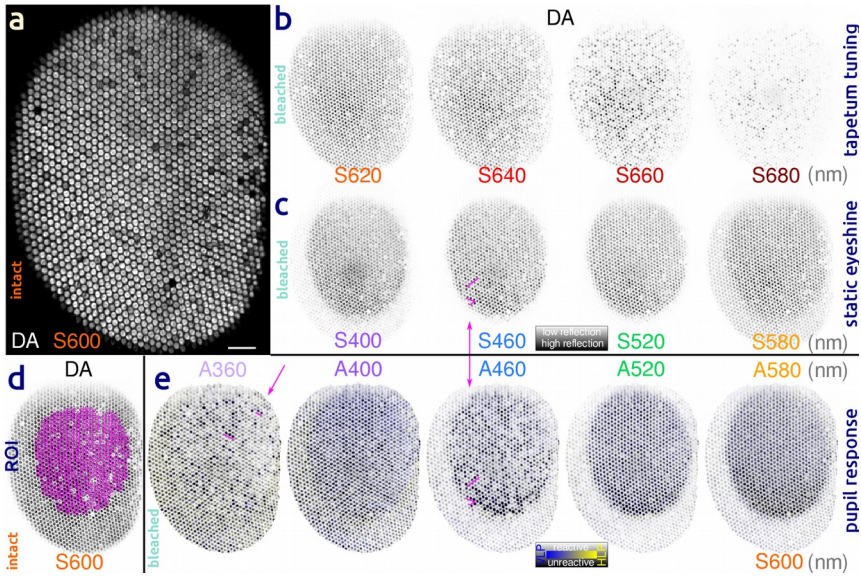

Figure 5. Eyeshine images, dependence on wavelength and bleaching. The images in panels b–e are shown inverted. **(a)** Dark adapted eyeshine at 600 nm in the unbleached eye. **(b)** Dark adapted eyeshine in the bleached eye in the red wavelength range. **(c)** Idem at lower wavelengths. **(d)** ROIs superimposed over the unbleached, dark adapted eyeshine. **(e)** The eyeshine vanishes due to light adaptation. Unreactive ommatidia appear dark. A few ommatidia do not react to UV light (360 nm) and about a half do not react to blue light (460 nm). All bleached ommatidia do not react to green light. In all images: DA – dark adapted. A – adapting wavelength (nm) S – snapshot wavelength (nm). Scale in (a) – approximately 100 µm

Pupil responses

Informed by these results, we chose 600 nm as the test wavelength for measuring the light-induced pupil responses. The ROI segments used for the analysis of individual ommatidia are indicated by the superimposed lattice (Fig. 5d, magenta). Figure 5e presents images taken at 600 nm after the eye was adapted with polarised light at wavelengths 360, 400, 460, 520 and 580 nm. For the sake of clarity, the images are shown inverted: the ommatidia that have not reacted to the adapting wavelength appear black. A mosaic with a few unreactive ommatidia in the bleached area can be appreciated after UV adaptation, and about a half of the ommatidia in the bleached area did not react to blue adapting light (Fig. 5e, A360, A460). On the other hand, the mosaic is quite uniform both at 400 nm and at 520 nm (Fig. 5e, A400, A520). The pupil reaction of bleached ommatidia at 580 nm is very small. A slight correspondence between the ommatidia not reacting to 460 nm light (Fig. 5e, A460) and those retaining static reflections at this wavelength (Fig. 5c, S460) may be appreciated (red arrows).

The images with responses to vertically- and horizontally-oriented linearly polarised (VLP, HLP) adapting light stimuli were mapped to the blue and yellow pseudo colour channels. The bluish and yellow-brown tints indicate the ommatidia that reacted more to VLP and HLP stimuli, respectively. We also note that the mosaic of bright static ommatidial reflections in the red wavelength range (Fig. 5b, S660) does not coincide

with the functional mosaics obtained with pupil reactions (Fig. 5e, A360, A460; see also the ommatidial type lattice presented below in Fig. 8c).

The change of the eyeshine pattern is a function of adapting light intensity

Illumination of the eye triggers the pupil mechanism, resulting in a reflection change. To assess the pupil response as a function of the illumination intensity, we selected a patch of 3×20 ommatidia in the images (Fig. 6a). The reflection decrease induced by green (560 nm) adapting light over a range of 4 log units of intensity, from $\log I = -4.0$ to $\log I = 0.0$, is very similar in the whole set of analysed ommatidia, indicating that at this wavelength, all ommatidia have a very similar pupil sensitivity. We obtained three replicates of averaged radiation patterns at each adapting intensity, by averaging the images of reflection patterns in the 1D spatial frequency (Fourier) space along the vertical pixel columns (SI Fig. S2).

Figure 6b shows the grand average radiation pattern, for $\log I = -4.0$ to 0.0, in steps of half a log unit. The dark-adapted reflection pattern, at $\log I = -4.0$ (Fig. 6b), can be readily understood as a superposition of the first and second waveguide mode patterns (see Fig. 3h). With increasing light adaptation, the central dip vanishes as the intensity of the doughnut-like pattern is diminished and, and subsequently the Gaussian-like reflection pattern fades to dark (Fig. 6b).

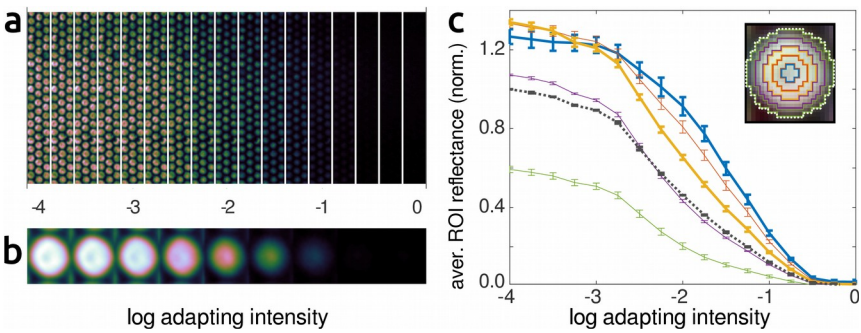

Figure 6. Pupil action on the eyeshine. (a) Raw images of 3 columns of 20 ommatidia, previously adapted with green (560 nm) light with intensities increasing in steps of 0.25 log unit. **(b)** Eyeshine pattern, average of the 60 ommatidia, resulting after adapting light flashes, increasing in steps of 0.5 log unit. **(c)** Average reflectance in circular annuli (ROIs) of the averaged eyeshine patterns as a function of adapting light intensity. The colours of the curves corresponds to the colour of the outer boundary of annuli shown in the inset. The dotted curve represents the reflectance for the total eyeshine pattern. Its dark-adapted value was used for normalising all reflectance data.

For all applied light intensities, we processed the reflection profiles by partitioning the averaged ommatidial image into concentric annuli around the profile's centre (Fig. 6c, inset). The dotted curve in Fig. 6c is the average reflectance of the total reflection pattern as a function of adapting light intensity, normalised to its dark-adapted value; this value was also used for normalisation of the data of the other curves. The blue curve of Fig. 6c represents the average reflectance within the smallest blue (jagged) circle as a function of the adapting light intensity, and the other curves represent the average reflectance in the annuli surrounding the central area. The curves of Fig. 6c

show that the pupillary response range spans about 4 log units of light intensity, in agreement with previous studies[40,45,46,47]. The annuli have different intensity dependencies of their reflectance curves. The reflectance in the outer ring (lowest, green curve in Fig. 6c), which represents primarily the pupillary action on the second order mode, falls much more rapidly between log$I$ = −3 and log$I$ = −1 than the reflectance in the centre of the pattern, which mostly depends on the first mode (Fig. 3h). This shows that the pupil first suppresses the second mode, and that at higher light intensities light waves propagating in the first mode are also extinguished.

Spectral and polarisation sensitivity of the ommatidial pupil

We investigated the sensitivity of the pupil mechanism in a large set of ommatidia by illuminating the central part of the butterfly eye with monochrome light flashes and subsequent measuring in each ommatidium the light-induced reflectance reduction at 600 nm. The adapting light was linearly polarised, oriented first vertically and then horizontally, i.e. parallel and perpendicular to the butterfly's symmetry plane, respectively. These two series of measurements were performed first on the dark-adapted, unbleached eye and subsequently after bleaching (SI Fig. S1a). By applying singular value decomposition, we identified three distinct ommatidial types (for details of the analysis, see SI Fig. S3). Figure 7 presents the average of the pupil sensitivity spectra for vertically- and horizontally-oriented polarised adapting light in the unbleached and bleached ommatidia belonging to the three ommatidial types.

In the sensitivity spectra three bands can be distinguished, peaking at 370 nm, 460 nm, and 520 nm. Their relative height specifically depends on the state of bleaching, which indicates that the activated pupil mechanisms exist in distinct UV, B, and G-sensitive photoreceptors. The ommatidial type UB (type I in *Papilio* and the honeybee) has three sensitivity peaks at 370, 460 and 520 nm, which we interpret to be due to one of the R1 and R2 photoreceptors being UV-sensitive and the other being blue-sensitive, while the other photoreceptors are all green receptors. The type UU (type II), has two clear sensitivity peaks, at 370 and 520 nm. The obvious interpretation is that in these ommatidia the photoreceptors R1 and R2 are both UV photoreceptors. In the type BB (type III), the UV peak is absent. This ommatidial type has overlapping blue and green peaks, meaning that both R1 and R2 are blue receptors and that they are joined again by the other photoreceptors being green receptors.

In all ommatidial types, the unbleached photoreceptors are more sensitive to vertically polarised stimuli (Fig. 7, solid curves) than to horizontally polarised stimuli (Fig. 7, dotted curves; see also SI Fig. S3c). In the UV range (<400 nm) the sensitivity difference is smaller than in the green wavelength range (>500 nm). In the bleached ommatidia (grey curves), compared to the unbleached ommatidia (coloured curves), the relative size of the green peak is clearly diminished, and the sensitivity differences to the polarised stimuli are smaller across the whole wavelength range. In the bleached BB ommatidia, polarisation sensitivity (PS) is about the same across the whole spectrum (Fig. 7), while in the bleached UU ommatidia, PS below 420 nm virtually disappears. This suggests that the UV photoreceptors are less polarisation sensitive than the blue-peaking photoreceptors.

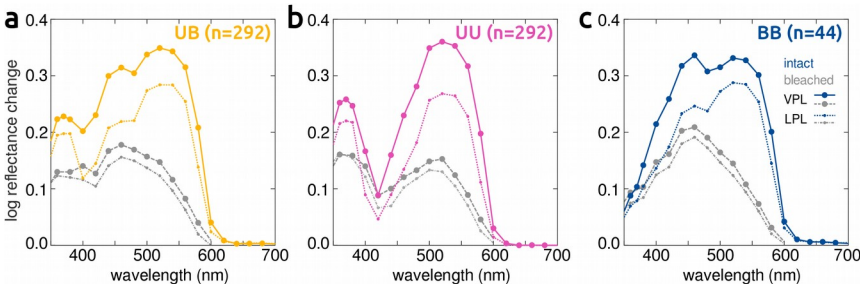

Figure 7. Pupil spectral sensitivity spectra of the three ommatidial types. (a) Response spectra of 292 UU-type ommatidia. **(b)** Response spectra of 292 UB-type ommatidia. **(c)** Response spectra of 44 BB-type ommatidia with two blue-peaking photoreceptors. The pupil sensitivity curves of the ommatidia in the unbleached eye (coloured solid and dotted curves) and after bleaching (grey dashed and dash-dotted curves) were obtained with 10 s pulses of equal intensity, monochromatic, linearly-polarised adapting light, oriented vertically (large symbols) and horizontally (small symbols). The data are the median of the log reflectance change (non-normalised).

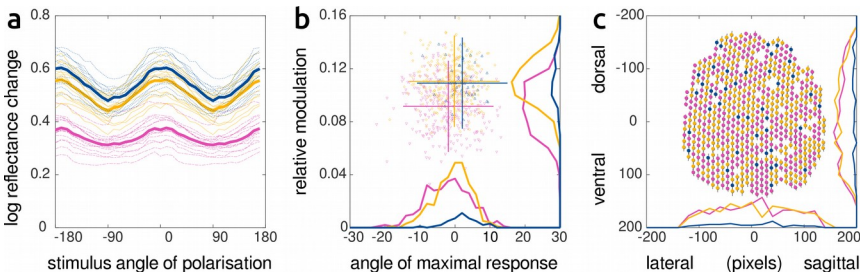

Figure 8. Pupil sensitivity to blue linearly polarised light (440 nm) and the allocation of the ommatidial types to the eye lattice. Colour coding: UU-type (*magenta*), UB-type (*yellow*), BB-type (*blue*). **(a)** Measurements of linear polarisation sensitivity of individual ommatidia (*thin stippled lines*) and the mean responses of the three ommatidial types (*thick lines*). **(b)** A scatterplot of relative modulation amplitude versus the corrected maximal response orientation. **(c)** Map of the maximal polarisation orientation (*short black lines*) showing a good correspondence with the local curvature of the lattice. The side histograms show the distribution of the three ommatidial types across the lattice.

We have tested the sensitivity of the pupil to the orientation of linearly polarised light in the intact eye, by measuring the pupil response to blue (440 nm) light flashes, linearly polarised with orientation changed in steps of 10° (Fig. 8). Calculation of modulation amplitude and phase was performed in the Fourier domain (see SI, Polarisation sensitivity analysis). All three ommatidial types appeared to be maximally sensitive to vertically-oriented, linearly-polarised blue light (Fig. 8a). All three types exhibit a relative modulation amplitude (0.07 to 0.14), corresponding to a polarisation sensitivity ratio of 1.15 to 1.32. Polarisation sensitivity is somewhat higher for the UB and BB ommatidial types than for the UU type (Fig. 8b). The local direction of maximal polarisation sensitivity only slightly deviates from the eye vertical direction (Fig. 8b), but the deviations closely correspond to the changes in the directions of the ommatidial lattice of the compound eyes (Fig. 8c).

Red admiral's red receptor?

Using the pupil mechanism as a diagnostic, we could identify three photoreceptor types, associated with the photoreceptors R1-8, in the eyes of *V. indica*. Because the R9 cell in Nymphalini butterflies does not contain pigment granules[27,38], it is likely not contributing to the pupil response. The functioning of the R9 cell remains obscure, but presumably its visual pigment is the same green rhodopsin that is expressed in cells R3-R8[41]. As the R9 photoreceptor is situated proximally in the retina, the light flux it receives for absorption is filtered by the visual pigments in the upper part of the rhabdom. We have modelled the spectral sensitivity of the photoreceptors in a UB ommatidium, specifically for the living light situation of a butterfly active in bright environments. The model computation is essentially the same as described previously[22,25].

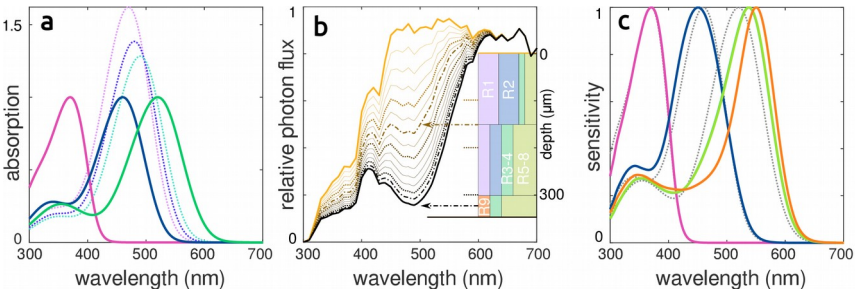

Figure 9. Modelling of the rhabdom in a UB-type ommatidium. (a) Template spectra of UV, blue and green rhodopsins peaking at 370, 450 and 520 nm (solid curves) and their metarhodopsins (dotted curves). Metarhodopsins have higher peak absorptions than the rhodopsins. (b) Reduction of the spectral photon flux as the light travels down the rhabdom. The fluxes at 100, 200, 300 µm depths (*dotted curves*) and at the boundaries of the three sections (*dash-dotted curves*) are emphasised. The fractional contributions of rhabdomeres are depicted in the *inset.* (c) Modelled spectral sensitivities of UV, blue, green and red photoreceptors (*coloured solid curves*) and their rhodopsin template spectra (*dotted curves*).

It should be stressed that the photochemistry of insect visual pigments is different from the visual pigments of vertebrates, namely that the rhodopsins are (inter) photoconvertible with a long-lived metarhodopsin state. The metarhodopsin state is, when in excess, slowly enzymatically degraded, a feature we employed for bleaching the green visual pigment. The absorption spectra of the rhodopsin/metarhodopsin pairs of the three concluded visual pigments are presented in Fig. 9a. When illuminated by normal daylight (D65), the visual pigments will reach a photosteady state, depending on the amount of absorbed light by the two pigment states. The model predicts metarhodopsin fractions of UV, B and G visual pigments under D65 illuminant to be about constant throughout the rhabdom depth, at ~0.2, ~0.4 and ~0.5, respectively (not shown).

The light flux in the rhabdom drops progressively with depth at shorter wavelengths, because of the absorption by the visual pigments in the rhabdom, but not in the long-wavelength range (Fig. 9b). The light flux in the long-wavelength range thus is specifically available for the proximal R9 cells, bringing about their red-shifted spectral

sensitivity. The normalised sensitivity spectra resulting from optical modelling are shown in Fig. 9c. The peak sensitivities of the UV photoreceptors, at 371 nm, is hardly different from the template. The peak sensitivity of the blue photoreceptor shifted from 460 to 451 nm, due to being screened by the metarhodopsins and the green rhodopsin. The peak of the photoreceptors R3-8 shifts from 520 to 538 nm, and the peak of the R9 photoreceptor shifts to 550 nm. The green receptors R3-8 and the 'red' – perhaps better 'yellow' – receptors R9 are thus predicted to be peaking 10~15 nm apart in the sunlight. For comparison, the peak sensitivities of human green and red cones differ by ~30 nm.

The modelled spectral sensitivity curves are calculated for sunlight conditions. In a fully dark adapted state with low metarhodopsin content, for instance, the sensitivity curve of green receptors is broader and has less red shift, while the modelled sensitivity curve of R9 gets a bilobed main peak (not shown). Owing to their small size and a large portion of light being absorbed distally, the light yield of photoreceptor R9 is in the range of a few percent, compared to that of R1-8. Photoreceptors compensate for the lower light yield with an increased transduction gain and a higher membrane resistance, yielding a longer time constant of the voltage response[55]. While the minute size of R9 clearly makes it a difficult electrophysiological target, larger photon bumps and a slower response at low and high light intensity stimulation, respectively, might be a better telltale sign than its erratic spectral sensitivity curve. 1

Conclusions

The Red admiral butterflies employ pigmentary and structural colouration on their wings to create both a cryptic brown pattern and a vivid blue-white-orange-black-pattern. The cryptic pattern on the lower wing is presumably used for camouflage during rest and hibernation, while the vivid upper wing pattern is likely used as a visual signal for intraspecific communication. The chemical and physical colouration mechanisms are typical of true butterflies: reflections from the wing scales with their lower lamina acting as a thin film reflector are either left unfiltered and appear white or blue, or get filtered by pigments and appear dark or red.

Complex colouration can be only appreciated with a sophisticated visual system, composed of a detector array with multiple spectral channels, arranged in a mosaic pattern, not unlike the Bayer pattern in colour cameras. On the other hand, the ommatidia also employ tiering (stacking) to modify the effective spectral sensitivity of the photoreceptors using the same green rhodopsin. A similar sensing principle is implemented in an image sensor (Foveon X3) with three stacked layers of silicon, where colour sensitivity is achieved without using coloured surface filters[56]. The rhabdom modelling suggests that in the eye of Nymphalini butterflies, this sensing principle may bring about the fourth, red-shifted photoreceptor type that presumably facilitates the detection of the red wing parts of the conspecifics. Hue discrimination is predicted to operate very well in the range between the peak sensitivities ~530 nm and ~550 nm of the two colour channels and a few tens of nanometres above[11], coinciding well with the red wing colour's reflectance increase between 550 and 600 nm. A similar case has been proposed for a diurnal moth with red colouration[28]. The solution of R9 being screened solely by metastable visual pigments seems to be limited by the achievable red shift and

by the dynamic changes of the spectral sensitivity curves due to the visual pigment photoequilibria involved. Inventing stable red perirhabdomal pigments turned out to be a prevailing solution for extending the red range in the majority of butterfly families[21,22,23,30,32].

Photoreceptors in the central part of the butterfly eye usually have low to moderate polarisation sensitivity; their physiological polarisation sensitivity ratio (PSR) is usually below 3. Nevertheless, Pieris can for instance use polarisation cues of the plant cuticles to augment its colour vision[21,59]. In nymphalid butterflies, the photoreceptors have PSR~1.8 (range 1.1~3.5) and the three morphological axes of green photoreceptor rhabdomeres are oriented ~60° from each other[27]. Our measurements of the compound pupil response expectedly report a lower PSR (1.2~1.5) in the blue-green part of the spectrum. In all ommatidia, the pupil responses were more sensitive to vertically polarised light, revealing a well aligned ommatidial lattice that allows for neuronal pooling. Put together, the triaxial arrangement of green photoreceptors within individual ommatidia and the possibility of signal pooling across neighbouring ommatidia might make the nymphalid retina a suitable system for unambiguous detection of weak polarised patterns in object-directed polarisation vision[21,55,58,59].

The ommatidial mosaic in butterfly eyes is presumably tuned to the visual ecology of the species and has possibly co-evolved with the colouration on butterfly wings and the butterfly visual environment. If object-directed polarisation vision is implemented in the neural circuits of nymphalid butterflies, its main function is likely to enhance general vision capabilities – for instance detecting surfaces during flight – rather than being specifically tuned to the colouration signals, which in the case of nymphalids, do not bear a significant polarisation pattern.

The mosaic in the mapped eye region of *Vanessa indica* appears to be random, the approximate ratio of the three ommatidial types is UB:UU:BB = 9:9:2. For comparison, the ratio in *Papilio* is 2:1:1[43]. The fractions of ommatidial types often have dorso-ventral gradients[30,32,41]. We should stress that a relatively small area, <10% of the *Vanessa's* visual field, was analysed in the presented experiments. About 1500 ommatidia could be sampled using the objective's full aperture (0.45), and if a larger visual world map is desired, an air objective with a larger aperture (NA 0.6~0.8) can be used, but at a price of image distortions and worse UV performance. Perhaps a better alternative is to automatise the goniometric positioner and the acquisition software.

We are barely beginning to understand the intricacies of the compound eye mosaic tuning, its physiological and behavioural benefits, and the underlying evolutionary mechanisms. Optical retinography (ORG) is a non-invasive method that makes possible long-term imaging and a deep functional analysis of visual systems, which reveals at once the spectral and polarisation properties of several hundred ommatidia and a few thousand contained photoreceptor cells, organized in intricate patterns. Both with extracellular electroretinography (ERG) and with ORG, the responses of individual photoreceptor cells have to be disentangled from the compounded responses. While single electrode ERG recordings are relatively simple to perform, they report a response from many photoreceptors in several ten to hundred ommatidia, so the results are difficult to interpret[60,61]. On the other hand, with ORG, the responses of ommatidia are

measured separately, virtually without any crosstalk. The ORG technique allows to map the compound eyes of butterflies with an unprecedented speed, opening up a path to a large scale comparative study of species, from which a picture of the variety of the functions of the ommatidial mosaic might start to emerge.

Acknowledgements

We wish to thank drs. Nicolas Nagloo and Yuri Ogawa for their insightful comments on the draft manuscript.

This study was financially supported by the Air Force Office of Scientific Research/ European Office of Aerospace Research and Development AFOSR/EOARD (grant FA9550-15-1-0068, to GB and DGS), JSPS KAKENHI (#18H05273 to KA) and jointly by the European Regional Development Fund (International Competitiveness of Research, Innovation and Technological Development) and MESS of R Slovenia (Early Career Researchers scheme, decision letter 5442-1/2018/434 to PP).

References

1. H. Ghiradella, *in Microscopic anatomy of invertebrates, Vol. 11A: Insecta*, ed. M. Locke, Wiley-Liss, New York, 1998, 257-287.
2. H. Ghiradella, *Adv. Insect Physiol.*, 2010, **38**, 135-180.
3. Y. Umebachi, *Zool. Sci.*, 1985, **2**, 163-174.
4. H. F. Nijhout, *The development and evolution of butterfly wing patterns*, Smithsonian Institution Press, Washington, 1991.
5. B. Wijnen, H. L. Leertouwer and D. G. Stavenga, *J. Insect Physiol.*, 2007, **53**, 1206-1217.
6. S. Kinoshita, *Structural colors in the realm of nature*, World Scientific, Singapore, 2008.
7. K. Michielsen, H. DeRaedt and D. G. Stavenga, *J. R. Soc. Interface*, 2010, **7**, 765-771.
8. D. G. Stavenga, H. L. Leertouwer and B. D. Wilts, *J. Exp. Biol.*, 2014, **217**, 2171-2180
9. M. A. Giraldo, S. Yoshioka, C. Liu and D. G. Stavenga, *J. Exp. Biol.*, 2016, **219**, 3936-3944
10. B. D. Wilts, B. A. Zubiri, M. A. Klatt, B. Butz, M. G. Fischer, S. T. Kelly, E. Spiecker, U. Steiner and G. E. Schröder-Turk, *Sci. Adv.*, 2017, **3**, e1603119.
11. H. Koshitaka, M. Kinoshita, M. Vorobyev and K. Arikawa, *Proc. R. Soc. London, Ser. B*, 2008, **275**, 947-954.
12. P. J. Chen, K. Arikawa and E. C. Yang, *PLoS One*, 2013, **8**, e62240
13. A. D. Briscoe and L. Chittka, *Annu. Rev. Entomol.*, 2001, **46**, 471-510.
14. M. Wakakuwa, D. G. Stavenga and K. Arikawa, *Photochem. Photobiol.*, 2007, **83**, 27-34.
15. S. M. Townson, B. S. Chang, E. Salcedo, L. V. Chadwell, N. E. Pierce and S. G. Britt, *J. Neurosci.*, 1998, **18**, 2412-2422.
16. G. D. Bernard and C. L. Remington, *Proc. Natl. Acad. Sci. USA*, 1991, **88**, 2783-2787.
17. D. G. Stavenga and K. Arikawa, *Arthropod Struct. Dev.*, 2006, **35**, 307-318.
18. A. D. Briscoe, S. M. Bybee, G. D. Bernard, F. Yuan, M. P. Sison-Mangus, R. D. Reed, A. D. Warren, J. Llorente-Bousquets and C. C. Chiao, *Proc. Natl. Acad. Sci. USA*, 2010, **107**, 3628-3633.
19. D. G. Stavenga, A. Matsushita and K. Arikawa, *Zool. Lett.*, 2015, **1**, 14.

20. D. G. Stavenga, H. L. Leertouwer, A. Meglič, K. Drašlar, M. F. Wehling, P. Pirih and G. Belušič, *PeerJ*, 2018, **6**, e4590.
21. A. J. Blake, P. Pirih, X. Qiu, K. Arikawa and G. Gries, *J. Comp. Physiol. A*, 2019, **205**, 553-565.
22. D. G. Stavenga and K. Arikawa, *J. Comp. Physiol. A*, 2011, **197**, 373-385.
23. K. Arikawa, *J. Comp. Physiol. A*, 2003, **189**, 791-800.
24. K. Arikawa, M. Wakakuwa, X. Qiu, M. Kurasawa and D. G. Stavenga, *J. Neurosci.*, 2005, **25**, 5935-5942.
25. Y. Ogawa, M. Kinoshita, D. G. Stavenga and K. Arikawa, *J. Exp. Biol.*, 2013, **216**, 1916-1923.
26. M. Kinoshita, M. Sato and K. Arikawa, *Naturwissenschaften*, 1997, **84**, 199-201.
27. N. Nagloo, M. Kinoshita and K. Arikawa, *J. Exp. Biol.*, 2020, **223**, 10.1242/jeb.217703
28. P. Pirih, M. Ilić, J. Rudolf, K. Arikawa, D.G. Stavenga and G. Belušič, *J. Comp. Physiol. A*, 2018, **204**, 639-651
29. W. H. Miller and G. D. Bernard, *J. Ultrastruct. Res.*, 1968, **24**, 286-294.
30. D. G. Stavenga, *J. Exp. Biol.*, 2002, **205**, 1077-1085.
31. X. Qiu, K. J. A. Vanhoutte, D. G. Stavenga and K. Arikawa, *Cell Tissue Res.*, 2002, **307**, 371-379.
32. D. G. Stavenga, *J. Comp. Physiol. A*, 2002, **188**, 337-348.
33. G. D. Bernard, *Science*, 1983, **219**, 69-71.
34. G. D. Bernard, *Science*, 1979, **203**, 1125-1127.
35. G. D. Bernard, *Biophys. Struct. Mech.*, 1983, **9**, 227-286.
36. K. J. A. Vanhoutte and D. G. Stavenga, *J. Comp. Physiol. A*, 2005, **191**, 461-473.
37. W. A. Ribi, *J. Comp. Physiol. A*, 1979, **132**, 1-9.
38. G. Kolb, *Zoomorphology*, 1985, **105**, 90-98
39. G. Kolb, *Zoomorphology*, 1986, **106**, 244-246.
40. D. G. Stavenga, J. A. J. Numan, J. Tinbergen and J. W. Kuiper, *J. Comp. Physiol. A*, 1977, **113**, 73-93.
41. A. D. Briscoe, G. D. Bernard, A. S. Szeto, L. M. Nagy and R. H. White, *J. Comp. Neurol.*, 2003, **458**, 334-349.
42. A. D. Briscoe and G. D. Bernard, *J. Exp. Biol.*, 2005, **208**, 687-696.
43. M. Perry, M. Kinoshita, G. Saldi, L. Huo, K. Arikawa and C. Desplan, *Nature*, 2016, **535**, 280-289
44. W. C. Gordon, *Z. Naturforsch. C*, 1977, **32**, 662-664.
45. D.-E. Nilsson, M. F. Land and J. Howard, *J. Comp. Physiol. A*, 1988, **162**, 341-366.
46. M. F. Land and D. C. Osorio, *Proc. R. Soc. London, Ser. B*, 1990, **241**, 93-100.
47. A. C. Järemo Jonson, M. F. Land, D. C. Osorio and D.-E. Nilsson, *J. Comp. Physiol. A*, 1998, **182**, 1-9.
48. M. Moody and J. Parriss, *Zeitschr. Vergl. Physiol.*, 1961, **44**, 268-291.
49. N. W. Roberts, M. L. Porter and T. W. Cronin, *Philos. Trans. R. Soc. London, Ser. B*, 2011, **366**, 627-637.
50. R. Wehner and G. D. Bernard, *Proc. Natl. Acad. Sci. USA*, 1993, **90**, 4132-4135.
51. J. Schindelin, I. Arganda-Carreras, E. Frise, V. Kaynig, M. Longair, T. Pietzsch, S. Preibisch, C. Rueden, S. Saalfeld and B. Schmid, *Nat. Methods*, 2012, **9**, 676-682.
52. I. Arganda-Carreras, C. O. Sorzano, R. Marabini, J. M. Carazo, C. Ortiz-de-Solorzano and J. Kybic, *Lect. Notes Comput. Sci.*, 2006, **4241**, 85-95.
53. P. Thevenaz, U. E. Ruttimann and M. Unser, *IEEE Trans. Image Process.*, 1998, **7**, 27-41.
54. J. W. Eaton, D. Bateman, S. Hauberg, R. Wehbring, GNU Octave (Version 5.2.0). GNU Project / Free Software Foundation, Boston, USA.
55. A. Meglič, M. Ilić, P. Pirih, A. Škorjanc, M. F. Wehling, M. Kreft, G. Belušič, *Proc. Natl. Acad. Sci. USA*, 2019. **116**, 21843-21853.
56. P. M. Hubel, J. Liu, and R. J. Guttosch, *Proc. SPIE*, **2004**, 5301, 402-407

57. M. J. How and N. J. Marshall. *Proc. R. Soc. London, Ser. B*, 2014, **281**, 20131632.
58. G. D. Bernard and R. Wehner, Vis. Res., 1977, **17**, 1019-1028.
59. A. J. Blake, M. C. Go, G. S. Hahn, H. Grey, S. Couture and G Gries. *Proc. R. Soc. London, Ser. B*, 2019, **286**, 20192198.
60. T. H. Goldsmith, *J. Comp. Physiol. A*, 1986, **159**, 481-487.
61. A. Steiner, R. Paul and R. Gemperlein, *J. Comp. Physiol. A*, 1987, **160**, 247-258.

Graphical abstract